Durable waterborne hydrophobic bio-epoxy coating with improved anti-icing and self-cleaning performance

Zheng, Shunli; Bellido-Aguilar, Daniel Angel; Wu, Xinghua; Zhan, Xuejun; Huang, Yinjuan; Zeng, Xianting; Zhang, Qichun; Chen, Zhong

2019

Zheng, S., Bellido-Aguilar, D. A., Wu, X., Zhan, X., Huang, Y., Zeng, X., . . . Chen, Z. (2018). Durable waterborne hydrophobic bio-epoxy coating with improved anti-icing and self-cleaning performance. ACS Sustainable Chemistry & Engineering, 7(1), 641-649. doi:10.1021/acssuschemeng.8b04203

https://hdl.handle.net/10356/143289

https://doi.org/10.1021/acssuschemeng.8b04203

Durable Waterborne Hydrophobic Bio-Epoxy Coating with Improved Anti-Icing and Self-Cleaning Performance

Shunli Zheng,[†] *Daniel Angel Bellido-Aguilar,*[†] *Xinghua Wu,*[†] *Xuejun Zhan,*[†] *Yinjuan Huang,*[†] *Xianting Zeng,*[‡] *Qichun Zhang,*[†] *Zhong Chen* [†,*]

[†] School of Materials Science and Engineering, Nanyang Technological University, 50 Nanyang Avenue, 639798, Singapore

[‡] Singapore Institute of Manufacturing Technology, 2 Fusionopolis Way, Singapore 138634

[*]**Corresponding Author:** Professor Zhong Chen

Email: ASZChen@ntu.edu.sg;

Tel: +65-67904256; Fax: +65-67909081

ABSTRACT: This study reports an environment-friendly waterborne hydrophobic bio-epoxy coating (WHBC), prepared by introducing dual-scale SiO_2 nanoparticles and (3-Glycidyloxypropyl) trimethoxysilane into an aqueous mixture containing the isosorbide based epoxy and a hydrophobic curing agent. The coatings were applied on Fe foil substrates using a one-step spin-coating method. The optimal coating with 33.3 wt.% SiO_2 nanoparticles exhibits high hydrophobicity with a water contact angle (CA) of 153.0 ± 1.1° and a sliding angle (SA) of 14.3 ± 1.9°. This optimal coating is found to have good mechanical durability against sand erosion. It maintained a high CA of 151.3 ± 2.0° and increased SA of 23.4 ± 3.7° after mechanical sandblasting for 30 s. The as-prepared optimal coating also showed excellent self-cleaning performance and was able to retain the good self-cleaning ability after the sandblasting. In addition, the as-obtained optimal coating shows a much lower icing temperature, a significantly longer icing delay time, and a low ice adhesion strength at 0.101 ± 0.019 MPa. The developed coating is bio-based and green, which holds various promising applications for marine, aerospace, energy harvesting and sports applications.

KEYWORDS: waterborne coatings, hydrophobic, bio-epoxy, durability, anti-icing, self-cleaning

INTRODUCTION

Epoxy resin has wide applications in coatings due to its excellent properties including superior chemical resistance, electrical insulating property, strong adhesion to various substrates, and good thermal stability.[1-3] To date, around 90% of the epoxy resin produced worldwide is diglycidyl ether of bisphenol A (DGEBA), which is derived from bisphenol A (BPA) and epichlorohydrin.[1, 4] BPA contributes more than 67% of the molar mass of DGEBA, and is mainly from fossil resources. After several-decades of investigation, it is proven that BPA is harmful to human health, especially on endocrine system.[5-6] Research indicates that BPA is estrogenic and may cause feminization

even at nanogram levels.[7] Moreover, it was shown that the increased temperature and the prolonged usage of BPA-based synthetic polymers speed up the hydrolysis of the corresponding polymer, due to the breakdown of the BPA-linked chemical bonds inside the polymer structures. Clearly, such degradation will cause more BPA release, leading to increasing toxicity to living organisms.[3, 8] Considering these adverse effects to human body, many countries have restricted the use of BPA in baby bottles, food packages and food related materials.[9] What's more, excessive consumption of BPA depletes fossil fuels, which is associated with the greenhouse gases emission and global warming.[10] Therefore, it is urgent to explore substitutes for BPA in synthesizing the epoxy resin.

Isosorbide, transformed from glucose, is a renewable and biodegradable material with similar reactivity structures to BPA, and holds promising chemical properties as well as attractive low price.[11] Isosorbide can be attached to glycidyl ether to formulate cross-linked bio-based epoxy resin monomers endowed with similar properties as DGEBA. Therefore, the conventional petroleum based DGEBA can be potentially replaced by isosorbide diglycidyl ether as the epoxy resin. This provides a unique opportunity to develop a new class of sustainable epoxy coatings. However, the high water absorption and the hydrophilic nature of epoxy resin have restricted its applications in certain working conditions such as heavy fouling and humid outdoor environments.[12-15] To overcome the problems, it is desirable to convert the hydrophilic nature of epoxy resin into hydrophobic through modification at molecular level, e.g., the incorporation of hydrophobic functional groups onto the epoxy molecules. In addition, isosorbide based epoxy resin tends to be mechanically weak, and the addition of inorganic nanoparticles could improve its mechanical properties.

Inspired by nature, mimicking lotus-leaf-like hydrophobic / superhydrophobic surfaces with non-sticking property has attracted considerable interest in both fundamental research and practical applications, including water proofing,[16-19] self-cleaning,[20-26] anti-icing,[27-34] corrosion resistance,[35-39] oil-water separation, [40-41] and drag reduction.[42-43] The realization of such surfaces is based on two important factors: low surface energy modification and rough surface construction. Several excellent works about the fabrication of hydrophobic / superhydrophobic epoxy coatings have been reported. For example, Zhang et al. created superhydrophobic fractal-structured particulate films using in-situ formed epoxy resin microspheres through phase separation in epoxy-amine curing system.[44] Guo et al.[45] and Ramesh et al.[46] reported a micro-nanoscale flowerlike ZnO/epoxy resin superhydrophobic coating and hydrophobic epoxy/PDMS composite coatings respectively by incorporating ZnO particles. Xin et al. produced hydrophobic epoxy coatings by incorporating a low-surface-energy benzoxazine monomer as the curing agent.[13] Li et al. achieved a hybrid superhydrophobic coating by embedding surface-modified dual-scale SiO_2 into fluorinated epoxy resin emulsion.[47] In addition, Psarski et al.[48] and Xiu et al.[49] produced superhydrophobic dual-sized filler epoxy composite coatings and mechanically-robust epoxy superhydrophobic surfaces through plasma treatment with surface fluorination. However, such processes tend to be more expensive due to the complicated procedure, the requirement of special equipment for substrate treatment, and the usage of expensive surface modification.

In addition, the aforementioned epoxy coatings are all prepared based on BPA, and most used solvents contain pungent or volatile organic compounds (VOCs), such as ethanol, acetone, xylene and toluene. These solvents are environmentally undesirable for a large-scale industrial production and can significantly increase the risks to human health. Thus, there are increasing interest and demand in the development of green epoxy resin coatings through an environmentally friendly

process. One of the possible approaches is to use bio-based epoxies that are processed in water rather than relying on VOCs. After the coating is formed, the surface should become hydrophobic or even superhydrophobic so that they are more resistant to contamination, corrosion and ice formation. Up to now, although a range of work based on the isosorbide based epoxy resin has been reported as the possible substitutes for the petroleum based epoxies,[3, 6, 50-51] most of the works focused on its synthesis, thermal property and thermomechanical property as the bulk polymers,[11, 52-54] work is rare to use bio-based materials for hydrophobic coatings with unique functionalities such as anti-icing and self-cleaning.

Herein, we reported an environmentally friendly waterborne hydrophobic coating using a mixture of bio-epoxy, hydrophobic Dynasylan® F 8815, dual-scale SiO_2 nanoparticles and (3-Glycidyloxypropyl) trimethoxysilane (GLYMO) in deionized (DI) water through a facile spin-coating method. SiO_2 nanoparticles embedded in epoxy contribute to the waterborne hydrophobic bio-epoxy coating (WHBC) by increasing the surface roughness as well as mechanical properties. GLYMO, a coupling agent, stabilizes the dispersion of SiO_2 in water and also enhances the adhesion of the coating to the substrate. Hydrophobic Dynasylan® F 8815 is used as a curing agent to form crosslinking polymer networks as well as to lower the surface energy. The optimal WHBC possesses a contact angle (CA) of 153.0 ± 1.1° and a sliding angle (SA) of 14.3 ±1.9° with 33.3 wt.% SiO_2 nanoparticles loading, showing high water repellency. The as-prepared optimal WHBC not only has excellent mechanical durability, but also impressive self-cleaning efficacy. Meanwhile, the coating also displays impressive improvement in the anti-icing performance.

EXPERIMENTAL SECTION

Sample Preparation. Fe foils (purity: 99.5%; thickness: 0.25 mm, Goodfellow Cambridge Limited, England) were mechanically polished with 1000 grit sandpaper and cut into small pieces (2.5 cm × 3 cm and 2.5 cm × 6 cm). These small pieces were ultrasonically degreased by ethanol and acetone before drying in air. A certain amount of (3-Glycidyloxypropyl) trimethoxysilane (GLYMO, purity ≥ 98%, Sigma-Aldrich, USA) was dropwise added into 4 g of deionized (DI) water with magnetic stirring at 375 rpm for 30 min. Next, two types of SiO_2 particles, 5-15 nm (spherical & porous) and 200 nm (mesoporous with pore size of 4 nm, Sigma-Aldrich, USA) in size, were dispersed by weight ratio of 2:1 in the GLYMO aqueous solution and stirred at 1200 rpm for 1 h. The mass ratio of GLYMO to SiO_2 was kept at 1:1. After that, 1 g of isosorbide-based bio-epoxy was blended inside the dispersion with vigorous stirring for another 1 h at 1200 rpm. The synthesis of isosorbide diglycidyl ether i.e., isosorbide based epoxy resin (as shown in the supporting information) followed a similar process reported in the literature by Chrysanthos et al.[3] (Figure S1). Finally, 2 g of hydrophobic curing agent of Dynasylan® F 8815 (Evonik Industries, Germany) was added and the reaction was allowed to proceed under constant stirring of 1200 rpm at room temperature for 24 h in order to reach a thorough mixing. 450 μL and 900 μL of the coating mixtures were respectively applied on 2.5 cm × 3 cm and 2.5 cm × 6 cm substrates. In order to keep a similar coating thickness for all the samples, the spin speed was controlled at 4000 rpm and 1000 rpm for the coating mixtures with and without SiO_2 nanoparticles under the same spin time of 30 s. The as-prepared coatings after adding different amount of SiO_2 (10, 20, 40, 50, 60 wt.% with respect to the epoxy and curing agent, which corresponds to 9.1, 16.7, 28.6, 33.3, 37.5 wt.% particle loading) are denoted as WHBC-10, WHBC-20, WHBC-40, WHBC-50 and WHBC-60, respectively. For comparison, the coating containing only isosorbide-based bio-epoxy and curing

agent was also prepared using the same heating process, and denoted as WHBC-0. The schematic fabrication process is shown in Figure S2.

Sample Characterization. OCA 20 contact angle measuring apparatus (DataPhysics Corporation, Germany) was used to measure the static and dynamic contact angles at room temperature. 5 μL and 10 μL of DI water were used for the CA and SA measurements, respectively. For each sample, at least 5 different locations were measured. The surface morphology and chemical composition were investigated using a field emission scanning electron microscope (FESEM, JEOL JSM-7600F, Japan) and the attached energy dispersive X-ray spectroscopy (EDS). The coating thickness and surface roughness with maximum scan length of 2000 μm was analyzed using a surface profiler (Alpha-Step IQ surface profiler, KLA Tencor). Fourier transform infrared spectroscopy (FTIR) run under the ATR mode was recorded by a FTIR spectrometer (PerkinElmer Inc.) to understand the molecular structures.

The coating adhesion to the substrates was estimated using a cross-cut tape adhesion tester according to ASTM D3359-09 standard by examining the cross-hatch patterns along the cut lines under an optical microscope (Olympus SZX16).

The mechanical durability was evaluated using a micro-sandblasting tester (LTH Machinery Pte Ltd, Singapore) based on ASTM F1864 test standard (Figure S3).

The ice adhesion test was carried out inside an ice chamber (Cincinnati Sub-Zero environmental chambers, USA) with an ice adhesion tester (Figure S4). The detailed procedure was reported in a previous study.[29] For each coating, at least 8 samples were tested and the arithmetic average value was reported as the ice adhesion strength.

The icing process of a water droplet placed on the sample surface was studied on the cooling stage of the contact angle measurement system with the aid of a built-in CCD camera. For the icing temperature measurement, the water droplet (5 μL) was dropped onto the sample surface and then cooled down. The temperature was reduced from room temperature to 0 ºC at 5 ºC/min, and at 1 ºC/min from 0 ºC till ice forms. While for the icing delay test, the water droplet (5 μL) was placed onto the sample surface after the temperature was decreased to -10 ºC. The time duration between the droplet onto the surface and the beginning of freezing was recorded as the icing delay time.

To evaluate the self-cleaning efficiency of the coatings, both dry carbon black powder and artificial dirt mixture were used as contaminants. The preparation of the artificial dirt mixture and the detailed procedure for the self-cleaning test are given in the supporting information.

RESULTS AND DISCUSSION

Contact Angle (CA), Sliding Angle (SA), Advancing Contact Angle (ACA), Receding Contact Angle (RCA), Roughness and Thickness of Different Samples. The CA and SA for different samples are shown in Table 1. CAs for the bare Fe substrate and smooth pure isosorbide based epoxy coating are 51.7 ± 2.0° and 50.0 ± 2.3°, respectively, indicating their hydrophilic nature. Whereas the Fe substrate coated with hydrophobic Dynasylan® F 8815 alone shows hydrophobicity with a CA of 110.2 ± 0.7°. CA increased slightly to 115.0 ± 0.7° for WHBC-0. However, the CA increased significantly after introducing the SiO_2 into the epoxy resin. When the amount of SiO_2 increased from 9.1 wt.% to 33.3 wt.%, the CA showed an obvious increase from 148.9 ± 2.1° for WHBC-10 to 153.0 ± 1.1° for WHBC-50 while the corresponding SA decreased from 32.4 ± 1.4° to 14.3 ± 1.9°. Further increasing SiO_2 content with 37.5 wt.% caused a slight decrease in CA (151.5 ± 1.1°) and sharp increase in SA (50.5 ± 3.0°) for WHBC-60. This can be attributed to the addition of a large amount of SiO_2 nanoparticles, which may not be fully covered

with the hydrophobic additive and thus some of the non-covered hydrophilic SiO_2 nanoparticles were exposed to the coating surface. This could result in the wetting mode transition from the Cassie-Baxter state to the Wenzel state. The change in contact angle hysteresis (CAH), i.e., the difference between ACA and RCA for different coatings matches well with the tendency of the SA. Thus, WHBC-50 has the maximum CA and minimum SA as well as CAH among all tested coatings with an optimal SiO_2 content at 33.3 wt.%. Besides, all the coatings show the similar thickness and the trend of surface roughness increases with particles loading (Table 1).

Table 1. CA, SA, ACA, RCA, roughness and thickness of different samples.

Samples	CA (°)	SA (°)	ACA (°)	RCA (°)	Roughness (nm)	Thickness (μm)
Fe	51.7 ± 2.0	> 90	—	—	—	—
Pure	50.0 ± 2.3	> 90	—	—	69.81 ± 12.03	1.58 ± 0.27
F8815	110.2 ± 0.7	> 90	122.6 ± 2.0	90.7 ± 1.5	61.94 ± 10.72	1.52 ± 0.12
WHBC-0	115.0 ± 0.7	> 90	122.7 ± 1.5	92.4 ± 2.3	95.59 ± 11.43	1.56 ± 0.31
WHBC-10	148.9 ± 2.1	32.4 ± 1.4	148.8 ± 1.5	133.8 ± 3.1	187.97 ± 20.06	1.61 ± 0.29
WHBC-20	150.1 ± 1.2	27.4 ± 5.3	149.8 ± 1.3	136.5 ± 2.4	224.88 ± 14.13	1.62 ± 0.22
WHBC-40	152.2 ± 1.2	24.4 ± 2.4	153.8 ± 3.0	143.8 ± 1.7	280.25 ± 16.56	1.62 ± 0.23
WHBC-50	153.0 ± 1.1	14.3 ± 1.9	154.4 ± 3.2	147.1 ± 2.2	313.84 ± 21.09	1.64 ± 0.16
WHBC-60	151.5 ± 1.1	50.5 ± 3.0	150.9 ± 1.1	130.2 ± 2.2	454.703 ± 0.72	1.71 ± 0.20

* "> 90" means the 10 μL of water droplet can't slide off from the sample surface even the surface is inclined to 90°.

To investigate the influence of stirring time on the coating wettability and adhesion, both CA and SA as well as optical microscope image after cross-cut tape adhesion test for the WHBC-50 coating are shown in Figure S5 and Figure S6. As an overall optimization among the different considerations, 24 h stirring is optimal for WHBC-50 due to its relatively higher hydrophobicity and the best coating adhesion (5 B). Detailed analysis is given in the supporting information.

The mirror-like phenomenon (Figure S7) is a good indication that surface wetting has been effectively prevented because of the low adhesion between water droplet and coating surface (Video S1). To visualize the interaction between them, we used a high speed camera (Vision Research, Phantom micro M120) to capture the dynamic moving process of water droplets on the sample surfaces (Video S2).

Surface Morphology and Chemical Composition. Roughness on two or more length scales has been suggested to be beneficial for a water-repellent surface. The creation of dual-scale surface roughness by introducing dual sized nanoparticles to achieve the unique wettability was reported by previous work.[55-57] The surface morphology is illustrated in Figure 1. The hydrophobic coating without adding SiO_2 (WHBC-0) is comparatively smooth while WHBC-50 consists of dense clustering of dual-scale nanoparticles that make the surface rough and porous. The porous structure on WHBC-50 can trap air inside and enable the observed strong water repellency. Coating cross-sections are shown in Figure S8. It is clear that the porous structures are distributed in the coating matrix [Figure S8(b_1) and (b_2)]. Besides, two coatings show a similar thickness around 1.6 μm [Figure S8(a_1) and (b_1)].

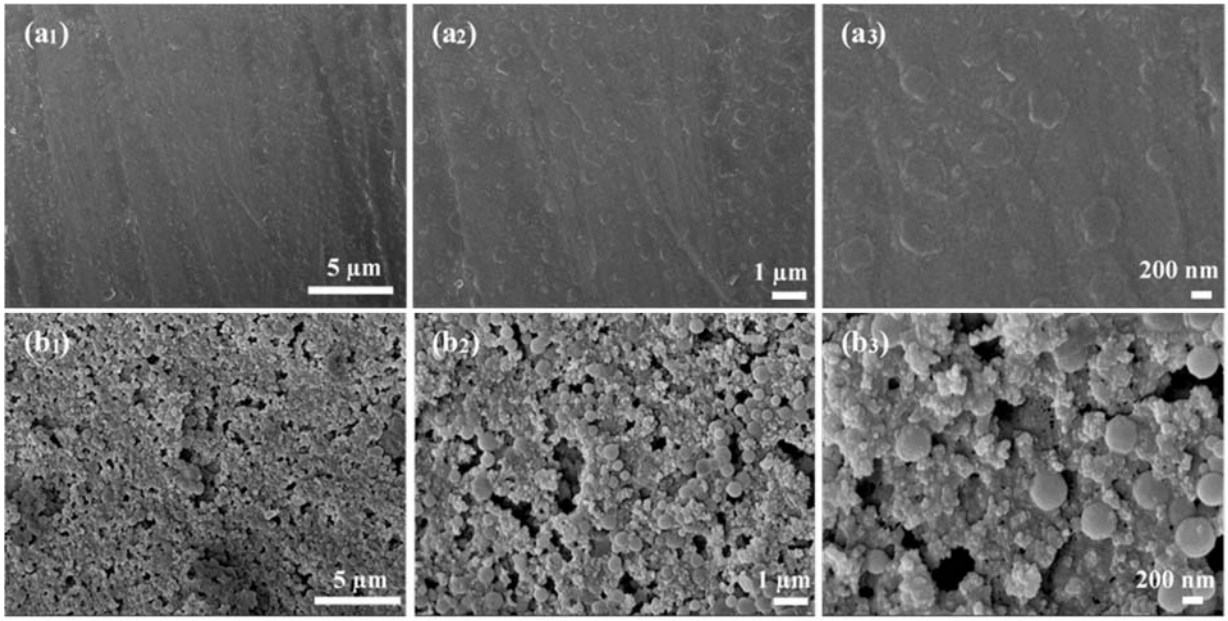

Figure 1. FESEM images of coatings with different magnification: (a_1-a_3) WHBC-0; (b_1-b_3) WHBC-50.

The coating formation reaction for WHBC-0 and WHBC-50 are suggested in Figure S9. Figure 2 shows the FTIR spectra of different samples. The absorption peak at 908 cm^{-1} and the broad peak at around 3458 cm^{-1} correspond to the vibration of epoxide group and –OH group respectively, confirming the successful synthesis of isosorbide based epoxy resin (spectrum a). For the commercial curing agent Dynasylan® F 8815, the characteristic absorption peaks appearing at 1206 cm^{-1} and 1237 cm^{-1} are assigned to C–F bond while the value at 1639 cm^{-1} is associated with –NH_2. In addition, the overlap of –OH and –NH_2 bands gives a much broader peak around 3000 - 3700 cm^{-1} (spectrum b). After the reaction (spectra c and d), the epoxide group disappears while the peak for C–F bond is present with a little shift for both WHBC-0 and WHBC-50. Besides, the peak intensity of –NH_2 (1652 cm^{-1} for WHBC-0 and 1645 cm^{-1} for WHBC-50) decreases and the broad peak between 3000 and 3700 cm^{-1} is absent with substitute of –OH peaks (around 3406 cm^{-1} for WHBC-0 and 3398 cm^{-1} for WHBC-50). The above results demonstrate that the aminolysis

reaction has occurred with complete consumption of isosorbide based epoxy resin. It is noted that there is no significant difference between the spectra of WHBC-0 and WHBC-50 except for the peaks at 794 cm^{-1} and 1037 cm^{-1} which are attributed to the SiO_2 nanoparticles.

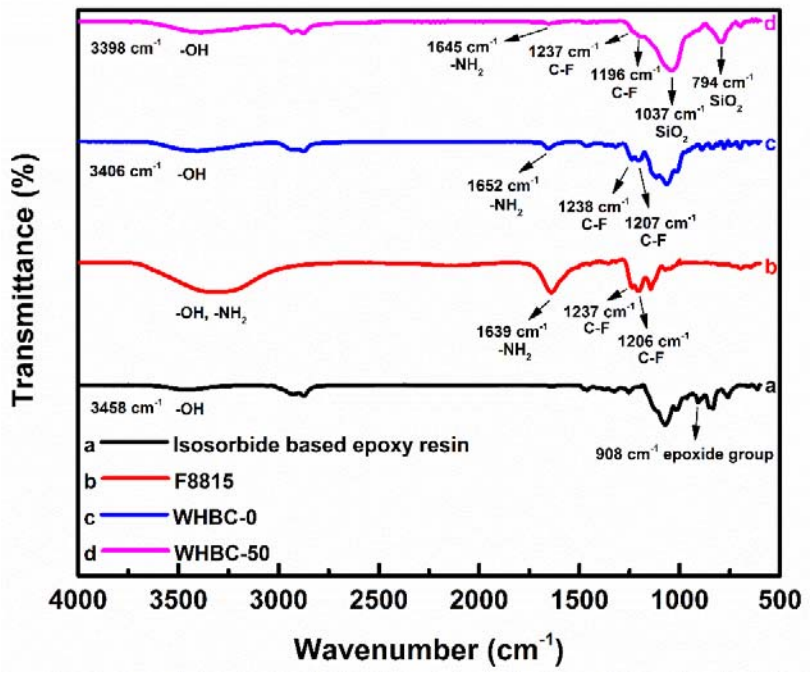

Figure 2. FTIR of different samples: (a) Isosorbide based epoxy resin; (b) Dynasylan® F 8815; (c) WHBC-0; (d) WHBC-50.

Wettability. The surface wettability is related to both surface structure and chemical composition.[58] The CA on the smooth isosorbide based bio-epoxy coating is 50.0 ± 2.3°, showing its hydrophilic nature. The CA increased to 115.0 ± 0.7° when the epoxy was mixed with hydrophobic curing agent Dynasylan® F 8815 (WHBC-0). The coating becomes highly hydrophobic with a CA of 153.0 ± 1.1° when 33.3 wt.% SiO_2 loading (WHBC-50). There are two possible wetting states with a high CA, *viz*., the Wenzel state and Cassie–Baxter state. Only the Cassie–Baxter state can result in a low SA.[59] Based on the current results, WHBC-50 is governed by the Cassie–Baxter equation:[60]

$$cos\theta_\gamma = f_1 cos\theta_1 + f_2 cos\theta_2 \qquad (1)$$

where θ_γ represents the measured apparent CA; f_1 and f_2 indicate the area fractions of solid surface (component 1) and air (component 2) on the composite coating surface; θ_1 and θ_2 are the corresponding intrinsic CAs of components 1 and 2 ($\theta_2 = 180°$). Since $f_1 + f_2 = 1$, equation (1) can be re-written as:

$$cos\theta_\gamma = f_1(cos\theta_1 + 1) - 1 \qquad (2)$$

According to the CAs on WHBC-0 and WHBC-50, the f_1 is estimated to be 0.19, which means the air occupies 81% of the water / coating interface. The above result demonstrates that the synergistic effect of both rough geometric structure and low surface energy material to construct the highly hydrophobic coating surface.

Ice Adhesion. As shown in Figure 3(a), there is a significant reduction in ice adhesion from 0.985 ± 0.195 MPa for the bare Fe substrate and 0.584 ± 0.068 MPa for the pure isosorbide based epoxy coating to 0.221 ± 0.065 MPa for the Dynasylan® F 8815 coating, 0.162 ± 0.053 MPa for WHBC-0, and 0.101 ± 0.019 MPa for WHBC-50. The noticeable change of ice adhesion strength for different samples can be attributed to their corresponding surface wettability. Due to the intrinsic hydrophilicity, both bare Fe and isosorbide based bio-epoxy coating surfaces can be fully wetted by water and adhesion with ice is relatively high. For the hydrophobic Dynasylan® F 8815 coating and WHBC-0, the ice adhesion was remarkably reduced as compared to that on the hydrophilic surfaces because their water repellency can reduce the moisture absorption and bonding between ice and coating surface. The WHBC-50 with a high degree of hydrophobicity shows the lowest ice adhesion among all the samples. Such low ice adhesion strength is attributed to the trapped air inside the porous coating structure. In addition to reducing the actual contact area

between ice and the substrate, the trapped air is able to prevent the water droplet from contacting the concave part on a rough coating surface, so the water can only rest on the top of convex region. It is known that the heterogeneous nucleation is more difficult on a convex surface than on flat or concave ones according to the classical nucleation theory.[61-63] Accordingly, it is difficult for ice to form on WHBC-50 surface. Furthermore, the entrapped air is compressed when water turns into ice. This would give rise to a relatively higher pressure to the ice, leading to a pre-stress on the ice to make it easier to be removed. As shown in Figure S10, plenty of ice was left on bare Fe surface after its removal while little can be seen on WHBC-50 surface.

The dynamic droplet impacting behavior was also studied to investigate the retained hydrophobicity of WHBC-50 after ice adhesion test (Video S3). After returning to ambient temperature, the water droplet can still bounce off from the coating surface, which means the coating has recovered to the Cassie-Baxter state with excellent non-wettability.

The durability of anti-icing function should also be taken into account as it directly affects the practical application of any coatings. Figure 3(b) and (c) shows the ice adhesion strength as well as CA and SA as a function of the number of ice removal cycles. It can be found that the ice adhesion of WHBC-50 does not change much after 10 cycles (0.113 ± 0.027 MPa), as indicated in Figure 3(b). In parallel, both CA and SA were also measured after repetitive ice removal tests on the coating surface, and the corresponding results are shown in Figure 3(c). There was a small decrease in CA and an increase in SA for WHBC-50, indicating certain degree of deterioration in its water repellency. Nonetheless, the coating remained highly hydrophobic, and the tendency of wettability is consistent with the slightly increased ice adhesion. To better understand these observations, the surface morphology and chemical composition were compared before and after 10 repetitive cycles (Figure S11). We found that there is no significant difference in the surface

morphology on WHBC-50 comparing with Figure 1(b_1-b_2), which means that the original porous structure survived after multiply ice removal cycles. Besides, the EDS composition analysis shows that the element F is largely preserved with a small amount of loss, which means the loss of hydrophobic Dynasylan® F 8815 molecules. This could be the reason to cause the increase in ice adhesion and SA. Despite that, the ice adhesion is still lower than that of WHBC-0, and much lower than that on bare Fe surface.

The micro-sandblasting test was used to estimate the mechanical endurance of WHBC-50. As shown in Table S1, both the CA and SA of WHBC-50 worsened from 153.0 ± 1.1° and 14.3 ± 1.9° to 151.3 ± 2.0° and 23.4 ± 3.7° with increasing sandblasting time. Nevertheless, the coating is still able to maintain the necessary water repellency after the sand erosion. As shown in Figure 3(d), the ice adhesion strength of WHBC-50 increased a little from 0.105 ± 0.011 MPa to 0.117 ± 0.011 MPa with the increasing sandblaster time from 5 s to 30 s. This is consistent with the trend in the wetting behavior. These results indicate that WHBC-50 possesses a reasonably good durability under the harsh erosive environment.

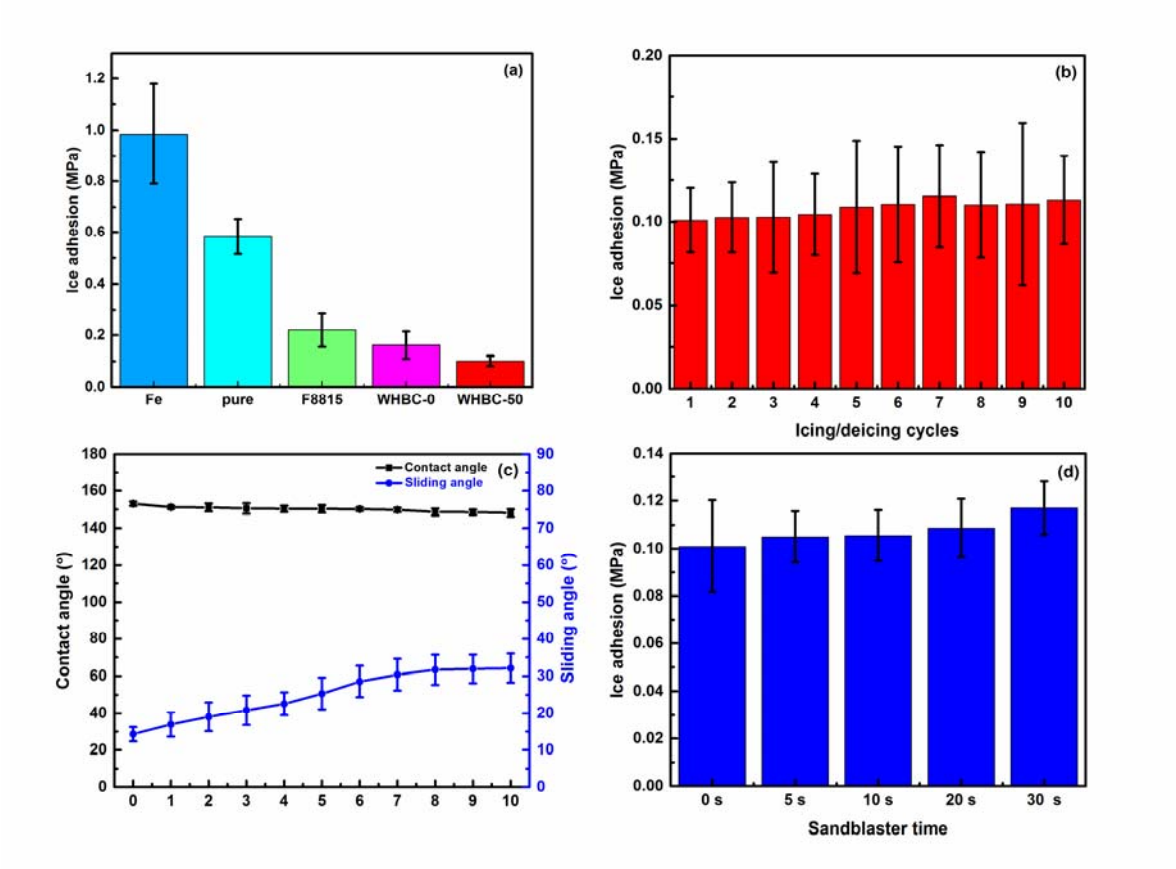

Figure 3. (a) Ice adhesion of different samples at -20 ºC for 24 h with relative humidity of 55 ± 3%; (b) The change of ice adhesion strength at -20 °C for WHBC-50 after different ice removal cycles; (c) CA and SA after the corresponding multiple cycles; (d) Ice adhesion strength at -20 °C for WHBC-50 after sandblaster treatment.

Icing Temperature. The icing temperature of water droplets on different samples were tested at a continuously cooling condition. The water droplets placed on WHBC-0 (hydrophobic) and WHBC-50 (highly hydrophobic) possess lower icing temperature of -16.5 °C and -21.3 °C as compared to that of -13.5 °C on the bare Fe substrate (hydrophilic). This can be explained by the combination of Kelvin's equation and Clausius–Clapeyron relation on a rough and porous surface structure in the case of WHBC-50, causing capillary formation.

The Kelvin's equation[64] is given as follows:

$$\ln\frac{p}{p_o} = \frac{2\gamma V_m}{RTr} \qquad (3)$$

where p and p_o are the vapour pressure and saturated vapour pressure at a certain temperature respectively; γ is the surface energy; V_m is the molar volume of phase; R is the gas constant; r is the radius curvature of droplet and T is the temperature. When a surface is intrinsically hydrophilic, the condensation of water would form a concave meniscus, which corresponds to a negative radius curvature of droplet. Consequently, $\ln\frac{p}{p_o}$ is negative ($p < p_o$). In the case of droplets on the intrinsically hydrophobic surfaces, the adjacent tri-junction between the water droplet and sample surface is considered as convex. The radius curvature of droplet is positive, leading to $p > p_o$. So it can be concluded that the value of r is related to the interface, thus can affect the p. Based on the analysis, p decreases when r decreases for a hydrophilic surface, while p increases when r decreases for a hydrophobic surface.

Combined with Clausius–Clapeyron relation,[32]

$$\frac{dp}{dT} = \frac{\Delta_\alpha^\beta H_m}{T\Delta_\alpha^\beta V_m} \qquad (4)$$

where p is vapour pressure; $\Delta_\alpha^\beta H_m$ and $\Delta_\alpha^\beta V_m$ are the enthalpy and volume difference from α phase to β phase respectively; T is the phase equilibrium temperature, i.e., the freezing temperature of the water droplet on the corresponding surface. After integration, we obtain equation (5) as follows.

$$\ln\frac{T_2}{T_1} = \frac{\Delta_{solidify}V_m}{\Delta_{solidify}H_m}(p_2 - p_1) \qquad (5)$$

As $\Delta V_m > 0$ and $\Delta H_m < 0$ during ice formation (solidification), there is a negative correlation between T and p.

Based on equations (3 - 5), the water droplets on the hydrophobic surfaces (WHBC-0 and WHBC-50) have higher pressures to supercool as compared with that on the hydrophilic surface (bare Fe substrate). Thus, the icing temperature is correspondingly decreased. Owing to the smaller r on WHBC-50, the water droplet on it tends to freeze at an even lower temperature.

Icing Delay. Figure 4 shows the icing process of water droplets on the bare Fe substrate and WHBC-50 respectively at -10 °C. The icing delay time can be determined according to the time when the transparency of the water droplet is lost due to the difference in light reflection between the water and ice.[65] The droplets on two surfaces are transparent initially (t = 0 s). With increasing time, the droplet on the bare Fe substrate became blurred and non-transparent after 78 s and 82 s, which implies the water started to freeze and was completely frozen at the respective times. In contrast, the droplet on WHBC-50 began to freeze after 1175 s and was frozen totally after 1198 s. It is obvious that the droplet on WHBC-50 takes much longer time to freeze, indicating its high anti-icing potential. It is worth mentioning that the water droplet changes on WHBC-50 from spherical shape to hemisphere when the temperature reaches -10 °C, which means the coating was partially wetted and not able to maintain the Cassie-Baxter mode entirely. Despite that, WHBC-50 can effectively delay ice formation in this partially wetted state due to the remaining trapped air. The above phenomenon can be well explained from the thermodynamics. The droplet on the sample surface can be considered as a system of solid-liquid-air three-phase interfaces. At a low temperature condition, it loses heat to the cold sample surface through contact heat conduction and thermal radiation. Meanwhile, it gains heat from air in the same forms of contact heat conduction and thermal radiation. The heat loss for the droplet per unit time can be expressed as:

$$\Delta h = h_l + h_{l'} - h_g - h_{g'} \qquad (6)$$

where h_l and $h_{l'}$ are the heat loss while h_g and $h_{g'}$ are the heat gains through the contact heat conduction and thermal radiation per unit time; Δh is the net heat loss in unit time. Accordingly, the time for the droplet to completely freeze on the sample surface can be expressed as:[66]

$$\Delta t = \frac{\rho_w C_P (T_o - T_s)}{\Delta h} \qquad (7)$$

where ρ_w is the water density; C_P is the heat capacity of pure water at constant pressure; T_o and T_s are the initial temperature of water droplet and sample surface temperature, respectively. It indicates that the smaller the Δh, the larger the Δt. The liquid-solid contact area on WHBC-50 is lower than that on the bare Fe substrate because of the remaining trapped air inside WHBC-50 at the subzero temperature, which causes less heat to lose, i.e., $h_{l(WHBC-50)} + h_{l'(WHBC-50)} < h_{l(Fe)} + h_{l'(Fe)}$. The lower liquid-solid contact area results in a higher contact area between liquid and air interfaces, which means larger heat gains from the air. Thus, the heat gain for WHBC-50 is higher: $h_{g(WHBC-50)} + h_{g'(WHBC-50)} > h_{g(Fe)} + h_{g'(Fe)}$. As stated above, the $\Delta h_{(WHBC-50)}$ is smaller than $\Delta h_{(Fe)}$, the $\Delta t_{(WHBC-50)}$ is correspondingly longer than $\Delta t_{(Fe)}$.

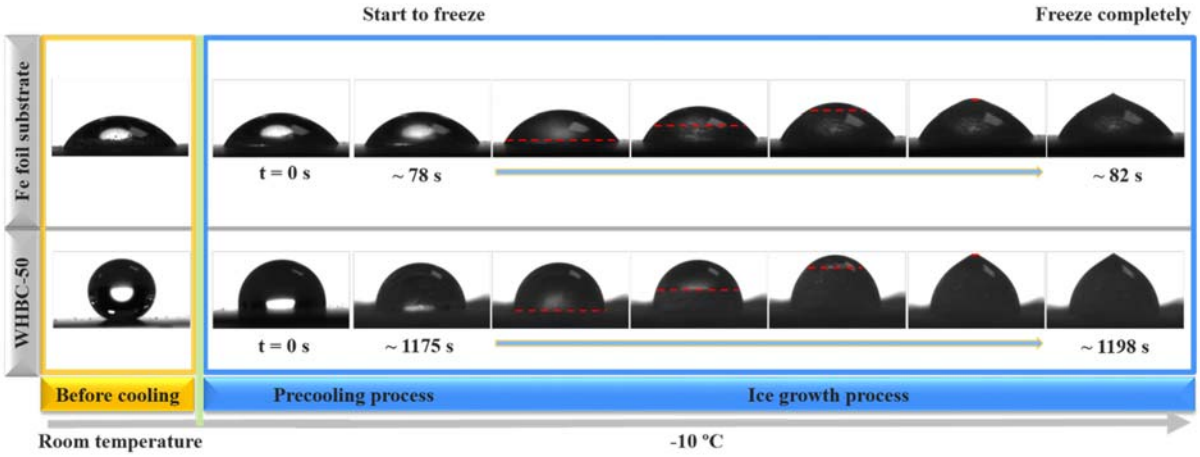

Figure 4. The icing process for 5 μL of water droplet on the bare Fe substrate and WHBC-50.

Self-cleaning Performance. The carbon black was used as dry contaminants for the self-cleaning test. The self-cleaning process is indicated in Figure 5. All the samples were placed at a tilt angle about 5º with horizontal plane and sprinkled with a sparse layer of carbon powder, as show in Figure 5(a_1)(b_1)(c_1). When the water droplets were dripped onto the contaminated surfaces, the carbon black powder adhered to both bare Fe [Figure 5(a_2-a_4)] and WHBC-0 [Figure 5(b_2-b_4)] surfaces. With continued water dripping, some powder on WHBC-0 surface was taken away but there was some water left [Figure 5(b_5)]. Under the same cleaning condition, there was a lot of powder residue on the bare Fe substrate [Figure 5(a_5)]. In contrary, the powder was easily removed from WHBC-50 after the same cleaning action [Figure 5(c_5)]. This phenomenon can be attributed to the joint action of high capillary forces induced by water droplets and weak adhesion of the contaminants to WHBC-50.[67] The detailed self-cleaning process is shown in Video S4.

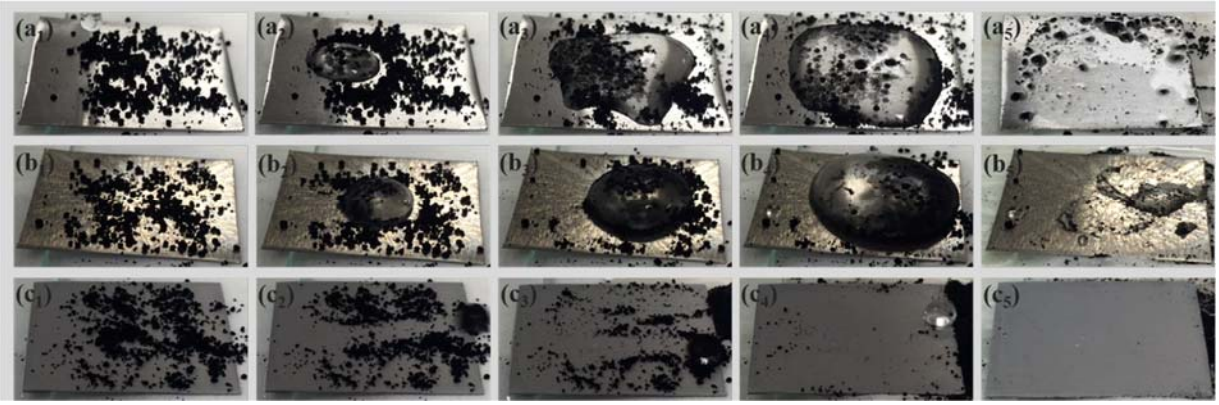

Figure 5. Self-cleaning process of different samples: (a_1-a_5) Fe foil substrate; (b_1-b_5) WHBC-0; (c_1-c_5) WHBC-50.

In order to quantify the self-cleaning efficiency of the as-prepared coatings, an artificial dirt mixture was applied as introduced before. Figure 6(a) shows the dirt accumulation before and after water spray cleaning on different samples, which changes from 48.3%, 23.3% and 8.0% to 41.7%, 11.1% and 2.0% on the Fe substrate, WHBC-0 and WHBC-50, respectively (Table S2). WHBC-

50 shows very lower dirt accumulation and retention as compared to those on bare Fe substrate and WHBC-0.

The corresponding images for the self-cleaning process is presented in Figure S12, which matches well with the results shown in Figure 6(a). The self-cleaning test was also performed on the coating after sandblasting treatment for different time to evaluate the coating's ability to remain self-cleaning after mechanical erosion. Despite slight increase in dirt accumulation, WHBC-50 still shows very low retention of dirt at about 5.3% after being sprayed-cleaned by water [Figure 6(b)] and remains highly self-cleaning at an efficiency of 94.7% [Figure 6(c)] after 30 s. The data are very similar to the initial values of 2.0% and 98.0% before sandblasting, showing good resistance to mechanical damage by WHBC-50. Detailed calculation and corresponding images are shown in Table S3 and Figure S13.

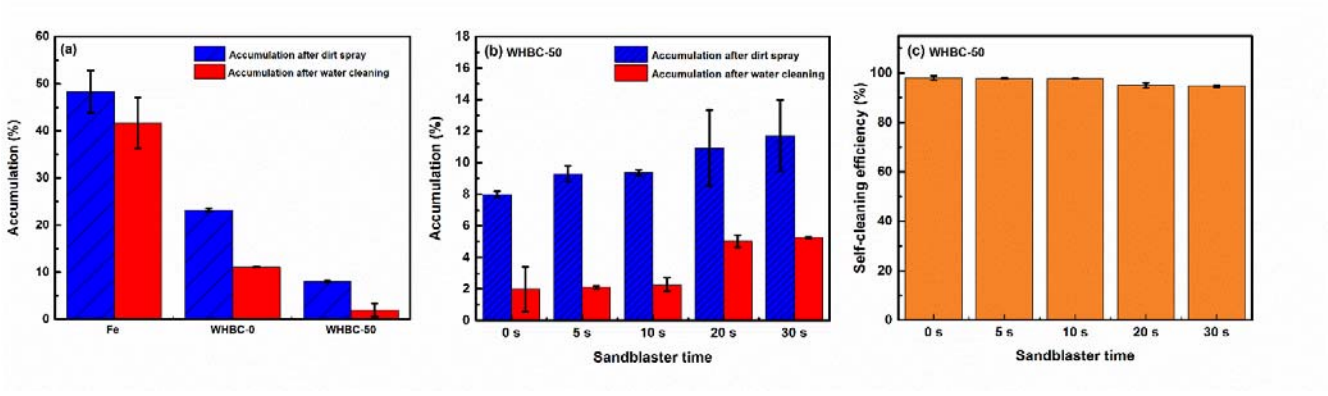

Figure 6. (a) Dirt accumulation on different samples before and after water spray cleaning; (b) Dirt accumulation and (c) Self-cleaning efficiency of WHBC-50 after sandblasting treatment for different time.

CONCLUSIONS

Eco-friendly waterborne coating was successfully prepared by introducing dual-scale SiO_2 nanoparticles into epoxy resin. The prepared coating shows a high level of hydrophobicity with a CA of 153.0 ± 1.1° and a SA of 14.3 ± 1.9°, derived from the synergy of rough surface structure and low surface energy. The optimal coating, WHBC-50 possesses a CA more than 150° after micro-sand sandblasting for 30 s, indicating good mechanical durability. Besides, WHBC-50 shows the lowest dirt accumulation and highest self-cleaning efficiency after the sand erosion. Furthermore, the as-prepared WHBC-50 demonstrates its improved anti-icing performance, displaying much reduced icing temperature, a longer icing delay time, and a lower ice adhesion strength. The bio-based coating is green and can provide a straightforward and effective way to fabricate highly hydrophobic coating on various substrates for large scale engineering applications.

ASSOCIATED CONTENT

Supporting Information

The Supporting Information is available free of charge on the ACS Publications website.

Additional figures and tables (PDF)

Video S1 (AVI)

Video S2 (AVI)

Video S3 (AVI)

Video S4 (AVI)

AUTHOR INFORMATION

Corresponding Author

*E-mail: ASZChen@ntu.edu.sg (Z.C.).

ORCID

Shunli Zheng: 0000-0002-4795-9388

Qichun Zhang: 0000-0003-1854-8659

Zhong Chen: 0000-0001-7518-1414

Notes

The authors declare no competing financial interest.

ACKNOWLEDGMENTS

The authors would like to thank the Agency for Science, Technology and Research (A*STAR) of Singapore (SERC 1528000048) for funding. We also thank Dr. Xin Zhao for the FESEM morphology observation.

REFERENCES

(1) Wan, J.; Gan, B.; Li, C.; Molina-Aldareguia, J.; Kalali, E. N.; Wang, X.; Wang, D.-Y. A Sustainable, Eugenol-Derived Epoxy Resin with High Biobased Content, Modulus, Hardness and Low Flammability: Synthesis, Curing Kinetics and Structure-Property Relationship. *Chem. Eng. J.* **2016,** *284*, 1080-1093, DOI org/10.1016/j.cej.2015.09.031.

(2) Ferdosian, F.; Zhang, Y.; Yuan, Z.; Anderson, M.; Xu, C. C. Curing Kinetics and Mechanical Properties of Bio-Based Epoxy Composites Comprising Lignin-Based Epoxy Resins. *Eur. Polym. J.* **2016,** *82*, 153-165, DOI org/10.1016/j.eurpolymj.2016.07.014.

(3) Chrysanthos, M.; Galy, J.; Pascault, J.-P. Preparation and Properties of Bio-Based Epoxy Networks Derived from Isosorbide Diglycidyl Ether. *Polymer* **2011,** *52*, 3611-3620, DOI org/10.1016/j.polymer.2011.06.001.

(4) Raquez, J.-M.; Deléglise, M.; Lacrampe, M.-F.; Krawczak, P. Thermosetting (Bio)materials Derived from Renewable Resources: a Critical Review. *Prog. Polym. Sci.* **2010,** *35*, 487-509, DOI org/10.1016/j.progpolymsci.2010.01.001.

(5) Ma, S.; Liu, X.; Jiang, Y.; Tang, Z.; Zhang, C.; Zhu, J. Bio-Based Epoxy Resin from Itaconic Acid and Its Thermosets Cured with Anhydride and Comonomers. *Green Chem.* **2013,** *15*, 245-254, DOI 10.1039/C2GC36715G.

(6) Łukaszczyk, J.; Janicki, B.; Kaczmarek, M. Synthesis and Properties of Isosorbide Based Epoxy Resin. *Eur. Polym. J.* **2011,** *47*, 1601-1606, DOI org/10.1016/j.eurpolymj.2011.05.009.

(7) Chapin, R. E.; Adams, J.; Boekelheide, K.; Gray, L. E.; Hayward, S. W.; Lees, P. S.; McIntyre, B. S.; Portier, K. M.; Schnorr, T. M.; Selevan, S. G. NTP-CERHR Expert Panel Report on the Reproductive and Developmental Toxicity of Bisphenol A. *Birth Defects Res., Part B: Dev. Reprod. Toxicol.* **2008,** *83*, 157-395, DOI org/10.1002/bdrb.20147.

(8) Michałowicz, J. Bisphenol A-Sources, Toxicity and Biotransformation. *Environ. Toxicol. Pharmacol.* **2014,** *37*, 738-758, DOI org/10.1016/j.etap.2014.02.003.

(9) Aouf, C.; Nouailhas, H.; Fache, M.; Caillol, S.; Boutevin, B.; Fulcrand, H. Multi-Functionalization of Gallic Acid. Synthesis of a Novel Bio-Based Epoxy Resin. *Eur. Polym. J.* **2013,** *49*, 1185-1195, DOI org/10.1016/j.eurpolymj.2012.11.025.

(10) Kanehashi, S.; Yokoyama, K.; Masuda, R.; Kidesaki, T.; Nagai, K.; Miyakoshi, T. Preparation and Characterization of Cardanol-Based Epoxy Resin for Coating at Room Temperature Curing. *J. Appl. Polym. Sci.* **2013,** *130*, 2468-2478, DOI org/10.1002/app.39382.

(11) Feng, X.; East, A.; Hammond, W.; Ophir, Z.; Zhang, Y.; Jaffe, M. Thermal Analysis Characterization of Isosorbide-Containing Thermosets: Isosorbide Epoxy as BPA Replacement for Thermosets Industry. *J. Therm. Anal. Calorim.* **2012,** *109*, 1267-1275, DOI 10.1007/s10973-012-2581-2.

(12) Wang, C.; Zuo, Y. Improvement of Surface and Moisture Resistance of Epoxy Resins with Fluorinated Glycidyl Ether. *J. Appl. Polym. Sci.* **2009,** *114*, 2528-2532, DOI org/10.1002/app.30803.

(13) Zhou, C.; Lu, X.; Xin, Z.; Liu, J.; Zhang, Y. Hydrophobic Benzoxazine-Cured Epoxy Coatings for Corrosion Protection. *Prog. Org. Coat.* **2013,** *76*, 1178-1183, DOI. org/10.1016/j.porgcoat.2013.03.013.

(14) Kumagai, S.; Xinsheng, W.; Yoshimura, N. Surface Degradation Phenomena of Outdoor Polymer Insulating Materials due to Acid Rain. *IEEJ Trans. Fund. Mater.* **1996,** *116*, 1121-1128, DOI org/10.1541/ieejfms1990.116.12_1121.

(15) Gubanski, S.; Hartings, R. Swedish Research on the Application of Composite Insulators in Outdoor Insulation. *IEEE Electr. Insul. Mag.* **1995,** *11*, 24-31, DOI 10.1109/57.466414.

(16) He, C.; Huang, J.; Li, S.; Meng, K.; Zhang, L.; Chen, Z.; Lai, Y. Mechanically Resistant and Sustainable Cellulose-Based Composite Aerogels with Excellent Flame Retardant, Sound-Absorption, and Superantiwetting Ability for Advanced Engineering Materials. *ACS Sustainable Chem. Eng.* **2018,** *6*, 927-936, DOI 10.1021/acssuschemeng.7b03281.

(17) Razavi, S. M. R.; Oh, J.; Sett, S.; Feng, L.; Yan, X.; Hoque, M. J.; Liu, A.; Haasch, R. T.; Masoomi, M.; Bagheri, R.; Miljkovic, N. Superhydrophobic Surfaces Made from Naturally Derived Hydrophobic Materials. *ACS Sustainable Chem. Eng.* **2017,** *5*, 11362-11370, DOI 10.1021/acssuschemeng.7b02424.

(18) Shen, Y.; Liu, S.; Zhu, C.; Tao, J.; Wang, G. Facile Fabrication of Hierarchical Structured Superhydrophobic Surface and Its Ultra Dynamic Water Repellency. *Chem. Eng. J.* **2017,** *313*, 47-55, DOI org/10.1016/j.cej.2016.12.063.

(19) Esmeryan, K. D.; Castano, C. E.; Bressler, A. H.; Abolghasemibizaki, M.; Mohammadi, R. Rapid Synthesis of Inherently Robust and Stable Superhydrophobic Carbon Soot Coatings. *Appl. Surf. Sci.* **2016,** *369*, 341-347, DOI org/10.1016/j.apsusc.2016.02.089.

(20) Wang, S.; Yu, X.; Zhang, Y. Large-Scale Fabrication of Translucent, Stretchable and Durable Superhydrophobic Composite Films. *J. Mater. Chem. A* **2017,** *5*, 23489-23496, DOI 10.1039/C7TA08203G.

(21) Kumar, D.; Wu, X.; Fu, Q.; Ho, J. W. C.; Kanhere, P. D.; Li, L.; Chen, Z. Hydrophobic Sol-Gel Coatings Based on Polydimethylsiloxane for Self-Cleaning Applications. *Mater. Des.* **2015,** *86*, 855-862, DOI org/10.1016/j.matdes.2015.07.174.

(22) Zheng, S.; Li, C.; Fu, Q.; Hu, W.; Xiang, T.; Wang, Q.; Du, M.; Liu, X.; Chen, Z. Development of Stable Superhydrophobic Coatings on Aluminum Surface for Corrosion-Resistant, Self-Cleaning, and Anti-Icing Applications. *Mater. Des.* **2016,** *93*, 261-270, DOI org/10.1016/j.matdes.2015.12.155.

(23) Chen, S.; Song, Y.; Xu, F. Highly Transparent and Hazy Cellulose Nanopaper Simultaneously with a Self-Cleaning Superhydrophobic Surface. *ACS Sustainable Chem. Eng.* **2018,** *6*, 5173-5181, DOI 10.1021/acssuschemeng.7b04814.

(24) Qing, Y.; Hu, C.; Yang, C.; An, K.; Tang, F.; Tan, J.; Liu, C. Rough Structure of Electrodeposition as a Template for an Ultrarobust Self-Cleaning Surface. *ACS Appl. Mater. Interfaces* **2017,** *9*, 16571-16580, DOI 10.1021/acsami.6b15745.

(25) Xie, W.-Y.; Song, F.; Wang, X.-L.; Wang, Y.-Z. Development of Copper Phosphate Nanoflowers on Soy Protein toward a Superhydrophobic and Self-Cleaning Film. *ACS Sustainable Chem. Eng.* **2017,** *5*, 869-875, DOI 10.1021/acssuschemeng.6b02199.

(26) Lu, Y.; Sathasivam, S.; Song, J.; Crick, C. R.; Carmalt, C. J.; Parkin, I. P. Robust Self-Cleaning Surfaces that Function When Exposed to either Air or Oil. *Science* **2015,** *347*, 1132-1135, DOI 10.1126/science.aaa0946.

(27) Wang, N.; Xiong, D.; Deng, Y.; Shi, Y.; Wang, K. Mechanically Robust Superhydrophobic Steel Surface with Anti-Icing, UV-Durability, and Corrosion Resistance Properties. *ACS Appl. Mater. Interfaces* **2015,** *7*, 6260-6272, DOI 10.1021/acsami.5b00558.

(28) Fu, Q.; Wu, X.; Kumar, D.; Ho, J. W.; Kanhere, P. D.; Srikanth, N.; Liu, E.; Wilson, P.; Chen, Z. Development of Sol-Gel Icephobic Coatings: Effect of Surface Roughness and Surface Energy. *ACS Appl. Mater. Interfaces* **2014,** *6*, 20685-20692, DOI 10.1021/am504348x.

(29) Zheng, S.; Li, C.; Fu, Q.; Xiang, T.; Hu, W.; Wang, J.; Ding, S.; Liu, P.; Chen, Z. Fabrication of a Micro-Nanostructured Superhydrophobic Aluminum Surface with Excellent Corrosion Resistance and Anti-Icing Performance. *RSC Adv.* **2016,** *6*, 79389-79400, DOI 10.1039/C6RA13447E.

(30) Kreder, M. J.; Alvarenga, J.; Kim, P.; Aizenberg, J. Design of Anti-Icing Surfaces: Smooth, Textured or Slippery? *Nat. Rev. Mater.* **2016,** *1*, 1-13, DOI 10.1038/natrevmats.2015.3.

(31) Wu, X.; Zheng, S.; Bellido-Aguilar, D. A.; Silberschmidt, V. V.; Chen, Z. Transparent Icephobic Coatings Using Bio-Based Epoxy Resin. *Mater. Des.* **2018,** *140*, 516-523, DOI org/10.1016/j.matdes.2017.12.017.

(32) Zhan, X.; Yan, Y.; Zhang, Q.; Chen, F. A Novel Superhydrophobic Hybrid Nanocomposite Material Prepared by Surface-Initiated AGET ATRP and Its Anti-Icing Properties. *J. Mater. Chem. A* **2014,** *2*, 9390-9399, DOI 10.1039/C4TA00634H.

(33) Wang, L.; Gong, Q.; Zhan, S.; Jiang, L.; Zheng, Y. Robust Anti-Icing Performance of a Flexible Superhydrophobic Surface. *Adv. Mater.* **2016,** *28*, 7729-7735, DOI org/10.1002/adma.201602480.

(34) Esmeryan, K. D.; Bressler, A. H.; Castano, C. E.; Fergusson, C. P.; Mohammadi, R. Rational Strategy for the Atmospheric Icing Prevention Based on Chemically Functionalized Carbon Soot Coatings. *Appl. Surf. Sci.* **2016,** *390*, 452-460, DOI org/10.1016/j.apsusc.2016.08.101.

(35) Zheng, S.; Li, C.; Fu, Q.; Li, M.; Hu, W.; Wang, Q.; Du, M.; Liu, X.; Chen, Z. Fabrication of Self-Cleaning Superhydrophobic Surface on Aluminum Alloys with Excellent Corrosion Resistance. *Surf. Coat. Technol.* **2015,** *276*, 341-348, DOI org/10.1016/j.surfcoat.2015.07.002.

(36) Feng, L.; Zhu, Y.; Wang, J.; Shi, X. One-step Hydrothermal Process to Fabricate Superhydrophobic Surface on Magnesium Alloy with Enhanced Corrosion Resistance and Self-cleaning Performance. *Appl. Surf. Sci.* **2017,** *422*, 566-573, DOI org/10.1016/j.apsusc.2017.06.066.

(37) Xiang, T.; Han, Y.; Guo, Z.; Wang, R.; Zheng, S.; Li, S.; Li, C.; Dai, X. Fabrication of Inherent Anticorrosion Superhydrophobic Surfaces on Metals. *ACS Sustainable Chem. Eng.* **2018,** *6*, 5598-5606, DOI 10.1021/acssuschemeng.8b00639.

(38) Peng, S.; Yang, X.; Tian, D.; Deng, W. Chemically Stable and Mechanically Durable Superamphiphobic Aluminum Surface with a Micro/Nanoscale Binary Structure. *ACS Appl. Mater. Interfaces* **2014,** *6*, 15188-15197, DOI 10.1021/am503441x.

(39) Xu, W.; Song, J.; Sun, J.; Lu, Y.; Yu, Z. Rapid Fabrication of Large-Area, Corrosion-Resistant Superhydrophobic Mg Alloy Surfaces. *ACS Appl. Mater. Interfaces* **2011,** *3*, 4404-4414, DOI 10.1021/am2010527.

(40) Wu, Y.; Jia, S.; Wang, S.; Qing, Y.; Yan, N.; Wang, Q.; Meng, T. A Facile and Novel Emulsion for Efficient and Convenient Fabrication of Durable Superhydrophobic Materials. *Chem. Eng. J.* **2017,** *328*, 186-196, DOI org/10.1016/j.cej.2017.07.023.

(41) Cheng, Q.-Y.; An, X.-P.; Li, Y.-D.; Huang, C.-L.; Zeng, J.-B. Sustainable and Biodegradable Superhydrophobic Coating from Epoxidized Soybean Oil and ZnO Nanoparticles on Cellulosic Substrates for Efficient Oil/Water Separation. *ACS Sustainable Chem. Eng.* **2017,** *5*, 11440-11450, DOI 10.1021/acssuschemeng.7b02549.

(42) Dong, H.; Cheng, M.; Zhang, Y.; Wei, H.; Shi, F. Extraordinary Drag-Reducing Effect of a Superhydrophobic Coating on a Macroscopic Model Ship at High Speed. *J. Mater. Chem. A* **2013,** *1*, 5886-5891, DOI 10.1039/C3TA10225D.

(43) Min, T.; Kim, J. Effects of Hydrophobic Surface on Skin-Friction Drag. *Phys. Fluids* **2004,** *16*, L55-L58, DOI org/10.1063/1.1755723.

(44) Quan, Y.-Y.; Zhang, L.-Z. Facile Fabrication of Superhydrophobic Films with Fractal Structures Using Epoxy Resin Microspheres. *Appl. Surf. Sci.* **2014,** *292*, 44-54, DOI org/10.1016/j.apsusc.2013.11.060.

(45) Zhang, X.; Si, Y.; Mo, J.; Guo, Z. Robust Micro-Nanoscale Flowerlike ZnO/Epoxy Resin Superhydrophobic Coating with Rapid Healing Ability. *Chem. Eng. J.* **2017,** *313*, 1152-1159, DOI org/10.1016/j.cej.2016.11.014.

(46) Ammar, S.; Ramesh, K.; Vengadaesvaran, B.; Ramesh, S.; Arof, A. Amelioration of Anticorrosion and Hydrophobic Properties of Epoxy/PDMS Composite Coatings Containing Nano ZnO Particles. *Prog. Org. Coat.* **2016,** *92*, 54-65, DOI org/10.1016/j.porgcoat.2015.12.007.

(47) Li, J. H.; Weng, R.; Di, X. Q.; Yao, Z. W. Gradient and Weather Resistant Hybrid Super-hydrophobic Coating Based on Fluorinated Epoxy Resin. *J. Appl. Polym. Sci.* **2014,** *131*, 40955, DOI org/10.1002/app.40955.

(48) Psarski, M.; Celichowski, G.; Marczak, J.; Gumowski, K.; Sobieraj, G. B. Superhydrophobic Dual-Sized Filler Epoxy Composite Coatings. *Surf. Coat. Technol.* **2013,** *225*, 66-74, DOI org/10.1016/j.surfcoat.2013.03.017.

(49) Xiu, Y.; Liu, Y.; Balu, B.; Hess, D. W.; Wong, C. Robust Superhydrophobic Surfaces Prepared with Epoxy Resin and Silica Nanoparticles. *IEEE Trans. Compon., Packag., Manuf. Technol.* **2012,** *2*, 395-401, DOI 10.1109/TCPMT.2011.2177088.

(50) Li, C.; Dai, J.; Liu, X.; Jiang, Y.; Ma, S.; Zhu, J. Green Synthesis of a Bio-Based Epoxy Curing Agent from Isosorbide in Aqueous Condition and Shape Memory Properties Investigation of the Cured Resin. *Macromol. Chem. Phys.* **2016,** *217*, 1439-1447, DOI org/10.1002/macp.201600055.

(51) Kumar, S.; Samal, S. K.; Mohanty, S.; Nayak, S. K. Recent Development of Biobased Epoxy Resins: a Review. *Polym.-Plast. Technol. Eng.* **2018,** *57*, 133-155, DOI org/10.1080/03602559.2016.1253742.

(52) Fleche, G.; Huchette, M. Isosorbide. Preparation, Properties and Chemistry. *Starch/Stärke* **1986,** *38*, 26-30, DOI org/10.1002/star.19860380107.

(53) Feng, X.; East, A. J.; Hammond, W.; Zhang, Y.; Jaffe, M. Overview of Advances in Sugar-Based Polymers. *Polym. Adv. Technol.* **2011,** *22*, 139-150, DOI org/10.1002/pat.1859.

(54) Sadler, J. M.; Toulan, F. R.; Nguyen, A.-P. T.; Kayea III, R. V.; Ziaee, S.; Palmese, G. R.; La Scala, J. J. Isosorbide as the Structural Component of Bio-Based Unsaturated Polyesters for Use as Thermosetting Resins. *Carbohydr. Polym.* **2014,** *100*, 97-106, DOI org/10.1016/j.carbpol.2013.04.036.

(55) Esteves, A.; Luo, Y.; van de Put, M. W.; Carcouët, C.; de With, G. Self-Replenishing Dual Structured Superhydrophobic Coatings Prepared by Drop-Casting of an All-in-One Dispersion. *Adv. Funct. Mater.* **2014,** *24*, 986-992, DOI org/10.1002/adfm.201301909.

(56) Karunakaran, R. G.; Lu, C.-H.; Zhang, Z.; Yang, S. Highly Transparent Superhydrophobic Surfaces from the Coassembly of Nanoparticles (≤ 100 nm). *Langmuir* **2011,** *27*, 4594-4602, DOI 10.1021/la104067c.

(57) Bravo, J.; Zhai, L.; Wu, Z.; Cohen, R. E.; Rubner, M. F. Transparent Superhydrophobic Films Based on Silica Nanoparticles. *Langmuir* **2007,** *23*, 7293-7298, DOI 10.1021/la070159q.

(58) Ji, H.; Chen, G.; Yang, J.; Hu, J.; Song, H.; Zhao, Y. A Simple Approach to Fabricate Stable Superhydrophobic Glass Surfaces. *Appl. Surf. Sci.* **2013,** *266*, 105-109, DOI org/10.1016/j.apsusc.2012.11.103.

(59) Liu, W.; Luo, Y.; Sun, L.; Wu, R.; Jiang, H.; Liu, Y. Fabrication of the Superhydrophobic Surface on Aluminum Alloy by Anodizing and Polymeric Coating. *Appl. Surf. Sci.* **2013,** *264*, 872-878, DOI org/10.1016/j.apsusc.2012.10.167.

(60) Cassie, A. B. D.; Baxter, S. Wettability of Porous Surfaces. *Trans. Faraday Soc.* **1944,** *40*, 546-551, DOI 10.1039/TF9444000546.

(61) Fletcher, N. Size Effect in Heterogeneous Nucleation. *J. Chem. Phys.* **1958,** *29*, 572-576, DOI org/10.1063/1.1744540.

(62) Xu, D.; Johnson, W. L. Geometric Model for the Critical-Value Problem of Nucleation Phenomena Containing the Size Effect of Nucleating Agent. *Phys. Rev. B* **2005,** *72*, 052101, DOI org/10.1103/PhysRevB.72.052101.

(63) Cooper, S. J.; Nicholson, C. E.; Liu, J. A Simple Classical Model for Predicting Onset Crystallization Temperatures on Curved Substrates and Its Implications for Phase Transitions in Confined Volumes. *J. Chem. Phys.* **2008,** *129*, 124715, DOI org/10.1063/1.2977993.

(64) Nosonovsky, M.; Bhushan, B. *Multiscale Dissipative Mechanisms and Hierarchical Surfaces: Friction, Superhydrophobicity, and Biomimetics*, Springer Science & Business Media: Berlin, 2008.

(65) Li, H.; Zhao, Y.; Yuan, X. Facile Preparation of Superhydrophobic Coating by Spraying a Pluorinated Acrylic Random Copolymer Micelle Solution. *Soft Matter* **2013,** *9*, 1005-1009, DOI 10.1039/C2SM26689J.

(66) Wen, M.; Wang, L.; Zhang, M.; Jiang, L.; Zheng, Y. Antifogging and Icing-Delay Properties of Composite Micro-and Nanostructured Surfaces. *ACS Appl. Mater. Interfaces* **2014,** *6*, 3963-3968, DOI 10.1021/am405232e.

(67) Su, F.; Yao, K. Facile Fabrication of Superhydrophobic Surface with Excellent Mechanical Abrasion and Corrosion Resistance on Copper Substrate by a Novel Method. *ACS Appl. Mater. Interfaces* **2014,** *6*, 8762-8770, DOI 10.1021/am501539b.

TOC/Abstract Graphic

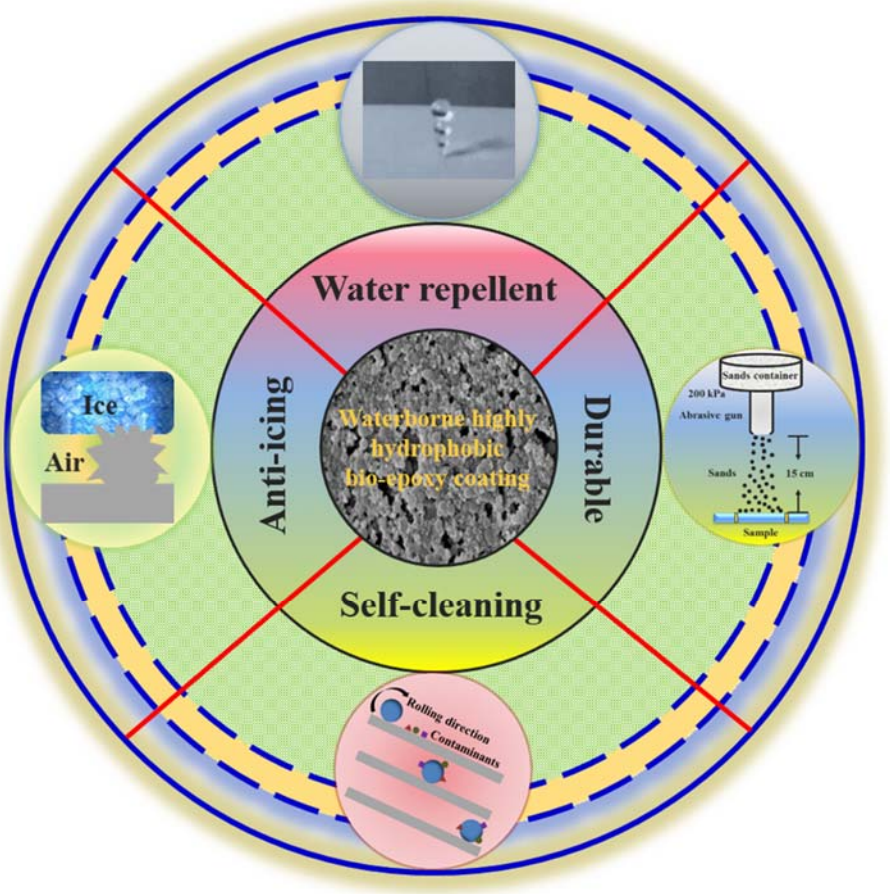

An environment-friendly waterborne hydrophobic bio-epoxy coating was successfully prepared by spin-coating method with mechanical durability, anti-icing and self-cleaning performance.